Airborne Autonomous Fault Detection for Shipboard Landing Navigation using Carrier Phase DGPS

Moon-Beom Heo and Boris Pervan
Department of Mechanical, Materials, and Aerospace Engineering, Illinois Institute of Technology

Sam Pullen, Jennifer Gautier, and Per Enge
Department of Aerospace and Astronautics, Stanford University

Demoz Gebre-Egziabher
Department of Aerospace Engineering & Mechanics, University of Minnesota

ABSTRACT

Shipboard-Relative GPS (SRGPS) is an architectural variant of the Joint Precision Approach and Landing System (JPALS) that is being developed to provide DGPS navigation for automatic shipboard landings in zero-visibility conditions. Unlike similar operations at ground-based airports, shipboard landing calls for higher navigation performance because of the mobility of the landing platform. The required vertical protection level for the navigation system is 1.1 m, with an associated integrity risk of approximately 10^{-7}. Under nominal signal conditions, it is desired that these integrity requirements be satisfied with a system availability of at least 99.7%. Because of the stringent nature of these specifications, carrier phase DGPS (CDGPS) solutions are being pursued.

This research is focused on the design of airborne integrity monitor algorithms to detect and isolate navigation threats that are undetectable by integrity monitors at the shipboard differential reference station. Such threats can be separated into two fundamental categories: (1) aircraft receiver failures, and (2) signal-in-space anomalies whose effects depend on the displacement between the user and the ship. For the carrier-phase-based SRGPS architecture, tracking loop cycle slips are the most obvious threats of the first category. Relevant threats that fall into the second class include ionospheric gradient and satellite orbit ephemeris anomalies. Airborne autonomous integrity monitoring algorithms designed to detect each of these threats are addressed in detail in this paper. The performance of the proposed integrity monitors is directly evaluated relative to the integrity requirements for aircraft shipboard landing navigation applications.

1. INTRODUCTION

In order to improve the accuracy and integrity of Standard Positioning Service (SPS), the differential GPS (DGPS) technique was conceived and developed [1, 2] in the early 1980s. The concept of DGPS is based on using the correlation in ranging errors between a reference station receiver and DGPS user receivers to eliminate co-existing ranging errors in the user ranging measurement. Ranging corrections are broadcast to all DGPS users in an operational service radius centered at the reference station. Use of differential ranging correction greatly improves accuracy and integrity for all DGPS users within the service radius. The Local Area Augmentation System (LAAS) is an example implementation of the DGPS concept [3]. LAAS is an aircraft precision landing navigation system being developed by the Federal Aviation Administration (FAA) with the objective to replace current Instrument Landing System (ILS). There are, however, some limitations to DGPS. Because the reference station is geographically separated from the user, the broadcast corrections are not the exact corrections for users' ranging errors. The differences between reference ranging corrections and user ranging errors are called differential ranging errors.

Shipboard-Relative GPS (SRGPS) is an architectural variant of the Joint Precision Approach and Landing System (JPALS) that is being developed to provide high accuracy and high integrity DGPS navigation for automatic shipboard landings. Unlike similar operations at ground-based airports, shipboard landing calls for higher navigation performance because of the mobility of the landing platform. The required vertical alert limit

(VAL) for the navigation system is 1.1 m, with an associated integrity risk of approximately 10^{-7}. [11] It is desired that these integrity requirements be satisfied with a system availability of at least 99.7% for nominal case when dual frequency signals are available. [12] The full availability of both L1 and L2 GPS signals for this military application is tempered by the simultaneous need to provide redundancy in the event of hostile jamming or interference. In the event of interference and jamming on one frequency, a target availability of 95% for single frequency navigation is assumed. Because of the stringent nature of these specifications, carrier phase DGPS (CDGPS) solutions are being pursued.

Centimeter-level navigation performance is possible with CDGPS because carrier ranging measurement errors are normally very small (typically subcentimeter), but the realization of this performance is dependent on the successful resolution of cycle ambiguities. The basic concept of CDGPS is that reference and user receive the signal from a given GPS satellite, and then the reference station broadcasts its measurement to the user. The user computes a 'single difference' phase by taking the difference between the user and reference carrier phase measurements time k for GPS satellite i. The mathematical expression of the single difference carrier phase is

$$\Delta\phi_k^i = -e_k^{i\,T} x_k + \tau_k + \lambda N^i + \nu_k^i \qquad (1)$$

where e_k is the line of sight (unit) vector to satellite i, x_k is the displacement vector from the reference station to the user, λ is the wavelength of carrier phase, N is the single difference cycle ambiguity (integer), τ_k is the single difference receiver clock bias, and ν is the single difference measurement error. When four or more satellites are in view, and cycle ambiguities are known, the user position can be estimated with respect to the reference station with centimeter-level accuracy. Example prior work on methodologies for cycle ambiguity resolution for aviation applications is given in [6, 7].

This research is focused on the design of airborne integrity monitor algorithms to detect and isolate navigation threats that are undetectable by integrity monitors at the shipboard differential reference station. (the development of shipboard integrity monitors is the subject of related concurrent work [13].) Such threats can be separated into two fundamental categories:

(1) Aircraft receiver failures.

(2) Signal-in-space anomalies whose effects depend on the displacement between the user and the ship.

For the CDGPS-based SRGPS navigation architecture, tracking loop cycle slips are the most obvious threats falling into the first category. Relevant threats of the second class include ionospheric gradient and satellite orbit ephemeris anomalies. These threats may be detectable by a ground-based reference facility because such a reference station can potentially be equipped with multiple reference antennas with long baselines. In contrast, SRGPS cannot detect these threats at the shipboard reference station because it will be equipped with either one reference antenna or multiple antennas with short baselines. In this paper, airborne autonomous integrity monitoring algorithms designed to detect each of these threats are addressed in detail. The performance of the proposed integrity monitors is directly evaluated relative to the navigation integrity requirements for shipboard landing of aircraft.

2. CYCLE SLIP DETECTION

The use of highly precise differential carrier phase measurements in SRGPS enables the high navigation performance required for shipboard landing. However, this performance is dependent on maintaining continuous phase lock on the carrier signals. Interference, jamming, shadowing, and high dynamics may cause loss of lock in the GPS receiver phase lock loops and result in a sudden integer cycle jump in the carrier phase observable. Such an event is known as cycle slip, and integrity is compromised when it is not detected. In this paper, the effectiveness of carrier phase Receiver Autonomous Integrity Monitoring (RAIM) [4,5] for cycle slip detection is explored. Single and multiple channel cycle slip threat models are considered for both single and dual frequency SRGPS architectures. The traditional RAIM concept is extended in this research by applying integer and half-integer constraints on failure magnitude. In addition, the availability of the RAIM-based cycle slip detection function is directly evaluated in this work.

2.1 Cycle Slip Threat Models

SRGPS can potentially operate in two different modes: a nominal dual frequency architecture and a single frequency backup when interference or jamming exists in either the L1 or L2 band. Single and multi-channel cycle slips are considered for both single and dual frequency architectures. The service availabilities of RAIM-based cycle slip detection of for the single and dual-frequency architectures are evaluated independently.

2.2 Single Frequency Architecture

For a single frequency processing architecture (operating on either L1 or L2 only, in the event of jamming or interference on the other frequency), it is possible to detect single channel cycle slips using carrier phase RAIM. A symbolic illustration of such a scenario is shown in the Figures 1a and 1b, which respectively show the nominal case of tracking six satellites in view and a cycle slip occurrence on channel 6.

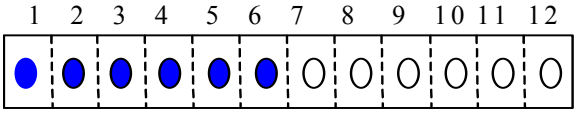

Figure 1a. Normal Condition.

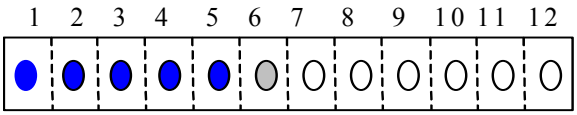

Figure 1b. Cycle Slip Occurs on a Single Channel.

In RAIM-based fault detection, a missed detection is said to occur when the position error exceeds the required alert limit but the least-squares residual is smaller than a predefined detection threshold. For SRGPS, the Vertical Alert Limit (VAL) is specified to be 1.1 m, and the detection threshold is defined to ensure a specified false alarm probability that is consistent with the continuity requirements for SRGPS. In this analysis, we assume a required false alarm probability of 10^{-7}.

The evaluation of RAIM-based cycle slip detection is facilitated by applying constraints on failure magnitude. It is assumed that the cycle slip occurs on the worst-case satellite channel with the worst-case bias of integer or half-integer magnitude.

Given a failure on a single satellite channel, the Failure Mode Slope (FMS) for the satellite is defined as the ratio of the vertical position error to the magnitude of residual vector. As illustrated in Figure 2, the normal measurement error dispersion (the 'ellipse' shown in the figure) can be envisioned to slide up and down along FMS depending on the failure magnitude. Because there exist multiple satellite measurements, there are multiple FMSs. Therefore, we consider the limiting case where the cycle slip occurs on the satellite channel with the steepest (worst-case) FMS.

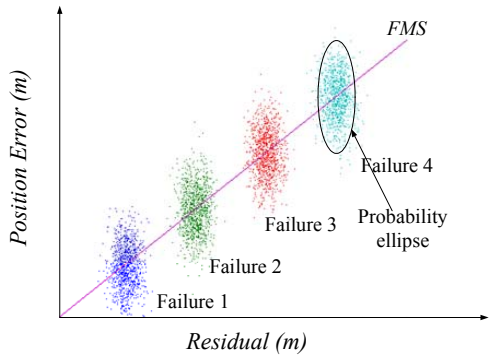

Figure 2. Failure Mode Slope

The worst-case failure magnitude can be found by increasing the failure magnitude by half cycle increments along the worst-case FMS. The probability of missed detection is computed at each increment, and the failure magnitude where the probability of missed detection is maximized is selected as the worst-case cycle slip.

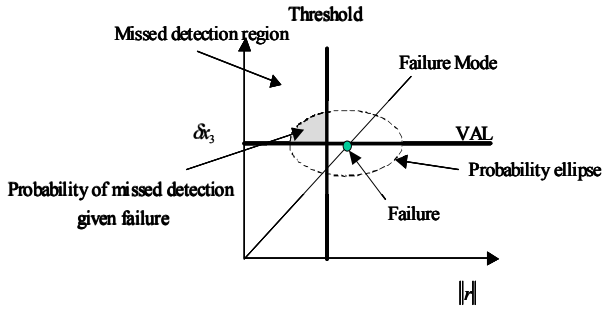

Figure 3. Probability of Missed Detection given Failure

The probability of missed detection, illustrated conceptually in Figure 3, is defined as the joint probability that the position error is larger than VAL and that the residual is smaller than the threshold. In the figure, and in the remainder of this paper, $\|r\|$ is the norm of the residual vector, and δx_3 is the vertical position error. In order to ensure navigation integrity using RAIM, the probability of missed detection must be lower than the ratio of the allocated integrity risk requirement and the prior probability of failure occurrence. In this work, we typically assume a required missed detection probability of 10^{-4}, but in the analysis that follows this value is varied as a parameter to observe its influence on overall performance. Given a missed detection probability requirement, the performance of RAIM-based cycle slip detection is quantified by its service *availability*.

2.2.1 Availability Analysis

Availability is defined as the fraction of time a navigation system is usable by the navigator. In the context of our RAIM analysis, a satellite geometry is declared unusable when the probability of missed detection of the worst-case cycle slip is larger than a prespecified minimum required to ensure integrity. RAIM availability is fundamentally limited by the 'raw' availability of having at least five satellites in view; this raw availability is the maximum theoretical RAIM availability a user can achieve.

In reality, the possibility of GPS satellite outages must also be considered in the computation of navigation service availability. In this case, service availability is a weighted average of conditional availabilities using GPS constellation state probabilities as the weighting factors. In this work, we use the Minimum Standard constellation state probability model defined in the GPS Standard Positioning Service Performance Specification [8].

2.2.2 Simulation Results

For a single frequency processing architecture, the service availability of carrier phase RAIM has been evaluated for the detection of full and half cycle slips on a single-channel. Figures 4a, 4b, and 4c quantify the sensitivity of RAIM availability to ship location. The RAIM availability results were computed for three different ship longitudes—Indian Ocean (60 deg E), Atlantic Ocean (-60 deg E) and Pacific Ocean (-135 deg E)—and latitudes varying from 5 deg N to 45 deg N. Each figure shows results for a constant longitude and variable latitude assuming a 7.5 deg elevation mask, a single difference measurement error standard deviation of 1 cm, and a required missed detection probability of 10^{-4}. In these figures, the colored bars represent, from left to right, the RAIM availability for detection of general failures with real-valued magnitude (dark blue), cycle slips of integer or half integer magnitude (light blue), cycle slips of integer magnitude (yellow), and the raw availability of having at least five satellites in view (red). The worst-case (lowest) service availability observed in the results occurs in Figure 4c (at 15 deg N, -135 deg E). It is clear, however, that even in this case, RAIM availability is higher than 97%, exceeding significantly the 95% target for single frequency operation. It is also evident in the results that minimal availability improvement is derived from the application of integer or half integer constraints on failure magnitude.

The sensitivity of RAIM availability to elevation mask is shown in Figure 5. The results in the figure were computed for the worst observed location found above, a

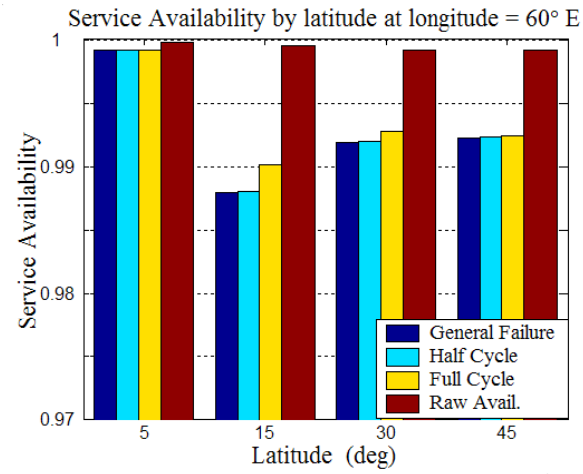

Figure 4a. Service Availability at Longitude = 60° E

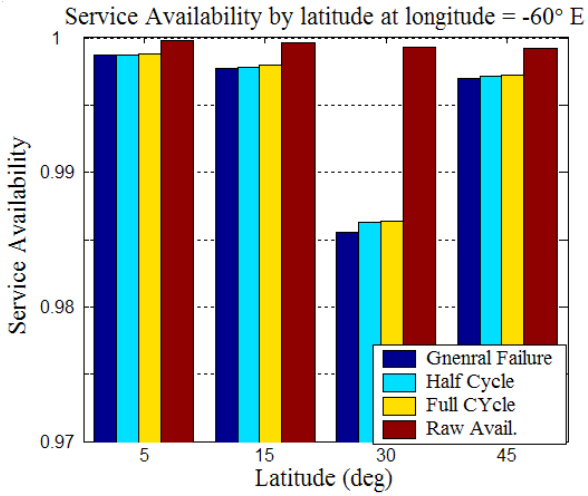

Figure 4b. Service Availability at Longitude = -60° E

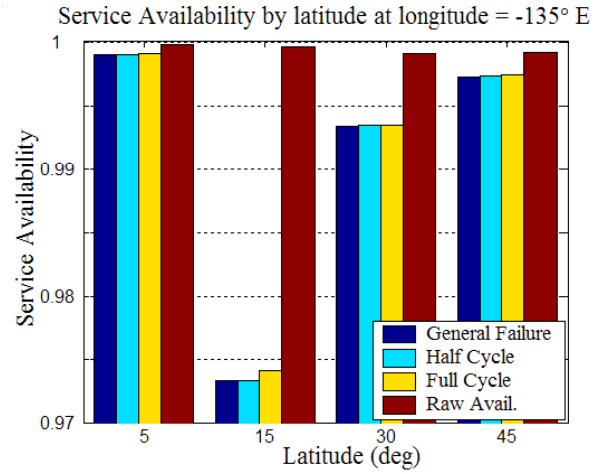

Figure 4c. Service Availability at Longitude = -135° E

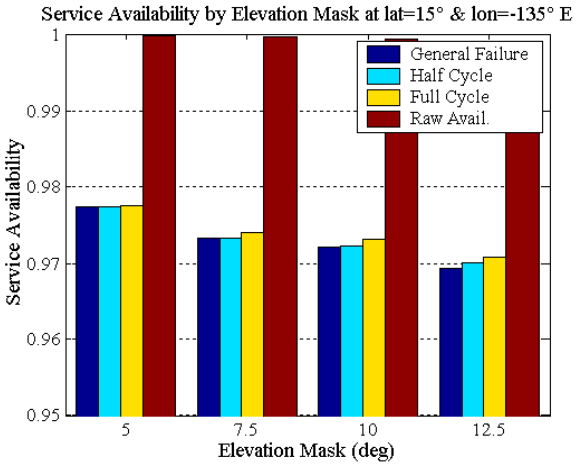

Figure 5. Service Availability vs. Elevation Mask

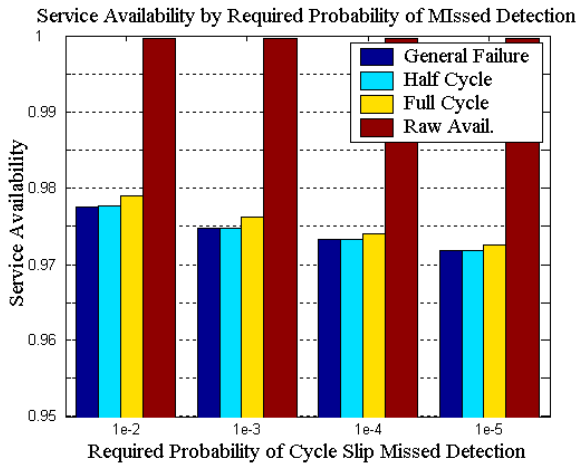

Figure 6. Service Availability vs. Required Probability of Cycle Slip Missed Detection

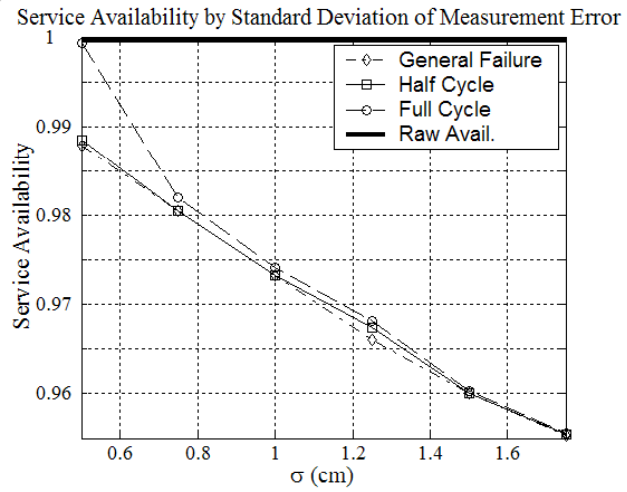

Figure 7. Availability vs. Measurement Error

required missed detection probability of 10^{-4}, and a single difference measurement error standard deviation of 1 cm. The results show that RAIM availability is moderately sensitive to elevation mask, but that a 95% target for single frequency operation is nevertheless easily achievable even for the highest elevation mask considered (12.5 deg).

The sensitivity of RAIM availability to required missed detection probability is shown in Figure 6. The results in the figure were computed for the worst observed location defined above, an elevation mask of 7.5 deg, and a single difference measurement error standard deviation of 1 cm. The results show that RAIM availability exhibits relatively weak sensitivity to required missed detection probability.

Finally, Figure 7 quantifies the sensitivity of RAIM availability to carrier phase measurement error standard deviation (σ). Again, the worst-case location, elevation mask of 7.5 deg, and required missed detection probability 10^{-4} were used. Smaller nominal measurement error allows tighter detection thresholds to be set, thereby reducing the number of satellite geometries that have missed detection probabilities higher than 10^{-4}. As a result RAIM availability is greater when measurement error standard deviation is lower. Service availability greater than 95% is achievable for values of σ up to 1.8 cm.

2.3 Dual Frequency Architecture

For a dual frequency processing architecture (the nominal operating mode for SRGPS), greater measurement redundancy exists for the detection of cycle slips. Figures 8a and b show an illustrative example of simultaneous multi-channel cycle slips in a dual frequency system.

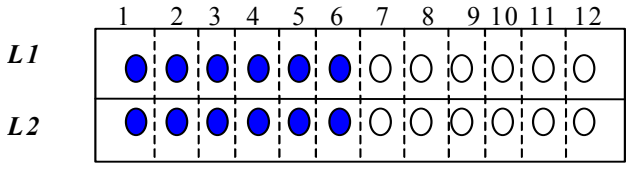

Figure 8a. Normal Conditions

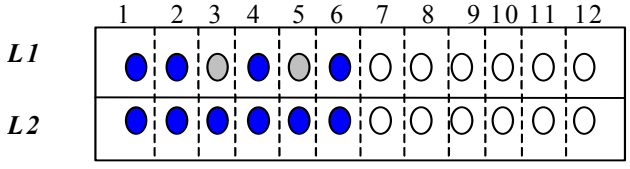

Figure 8b. Cycle Slips Occur on L1 Channels 3 and 5

We first consider the case where the cycle slips do not simultaneously occur on both frequencies for the same satellite. In this case, cycle slips can be detected by direct differencing of L1 and L2 differential ranging measurements:

$$\Delta\phi_{L1l2} = \phi_{L1} - \phi_{L2} = b + \Delta\nu \qquad (2)$$

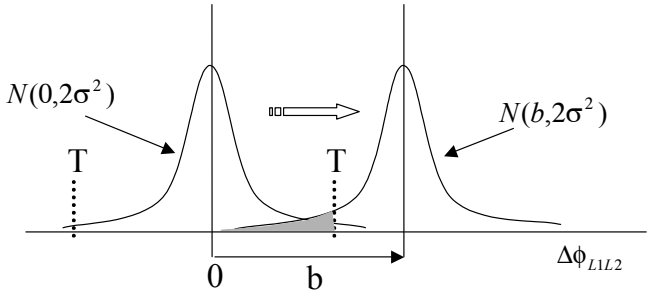

Figure 9. Differencing Between L1 and L2

where b is the bias due to the failure and $\Delta\nu$ is the nominal measurement error which is distributed as $\sim N(0,\sigma^2)$. Figure 9 illustrates a simple detection scenario where a threshold T is set such that, under normal error conditions, the probability of false alarm is sufficiently low to ensure navigation continuity. Given a failure, it is desired that the probability of missed detection be smaller than a certain required value to ensure integrity. For example, given a false alarm probability of 10^{-7} and σ = 1 cm, a missed detection probability of 10^{-4} can be ensured only if the magnitude of the bias (b) is greater than 0.128 m. Because the magnitude of a full cycle slip on L1 (19 cm) and L2 (24 cm) is always larger than the minimum detectable bias, the availability of the fault detection function using L1-L2 difference is 100% for full cycle slips. In contrast, half cycle slips (0.095 m for L1 and 0.12 m for L2) are smaller in magnitude than the minimum detectable bias, and therefore cannot be detected with the specified missed detection probability.

2.4 Summary of Cycle Slip Detection

The availability performance of autonomous cycle slip detection using redundant GPS measurements is encapsulated in Table 1. In summary, detection of cycle slips is guaranteed with the required availability for both single and dual frequency architectures provided that:

- for a single frequency architecture, slips do not simultaneously occur on multiple channels,
- for a dual frequency architecture, cycle slips are larger than a half integer in magnitude and do not simultaneously occur for the same satellite on both frequencies.

To ensure comprehensive detection of such events, inertial augmentation of the integrity monitor will likely be required [9,10].

	Single Frequency Algorithm		Dual Frequency Algorithm		
Required Service Availability	95%		99.7%		
Cycle Slip Occur	Single Channel	Multi Channel	Single Channel	Multi-Channel	
				Same SV	Diff-erent SVs
Half Cycle Slip	Yes	No	No*	No	No*
Full Cycle Slip	Yes	No	Yes	No	Yes

*RAIM is possible, but availability is lower than 99.7%.

Table 1. Summary of Cycle Slip Detection

3. EPHEMERIS ERROR DETECTION

Each satellite broadcasts its own orbit ephemeris so users can compute the satellite location at any time of interest. Because the satellite locations are used to calculate user position, an error in the satellite ephemeris will result in a navigation error. Under normal conditions these errors are negligibly small for differential GPS users, but integrity considerations for aircraft precision landing navigation dictate that *anomalous* conditions must be quickly detected. Furthermore, orbit ephemeris anomalies cause navigation errors that are dependent on the time-varying displacement between the aircraft and reference receiver. Therefore, the impact of potential orbit errors on navigation must ultimately be assessed separately by each individual aircraft within the SRGPS service volume. In this context, carrier phase RAIM is an attractive solution. The basis for observability of ephemeris failures using RAIM is that the magnitude of the residual test statistic will change proportionally during an approach as the distance between the aircraft and ship decreases. The effectiveness of such a 'relative' RAIM method is therefore dependent on the magnitude of the observed change in the test statistic, which in turn is dependent on total change in displacement during the approach within the SRGPS service radius.

Figure 10 is an illustration the basic concept. The 'Service Entry Point' is the radius where the aircraft is

first able to receive the reference measurements, and 'synthetic baseline' is the distance between service entry point and the aircraft location at any given time over the flight path. As the synthetic baseline increases, the ephemeris error will become detectable using relative RAIM. In this section, the autonomous ephemeris detection algorithm is described, and its effectiveness for SRGPS is evaluated.

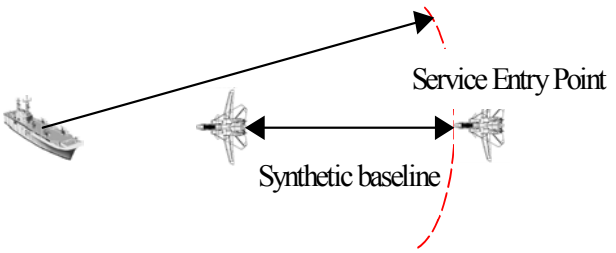

Figure 10. Service Entry Point and Synthetic Baseline

Because SRGPS uses carrier phase differential GPS, navigation performance is dependent on the successful resolution of cycle ambiguities corresponding to the GPS satellites in view. During measurement updates, the ephemeris error may affect the cycle ambiguity estimation process. In turn, incorrectly estimated cycle ambiguities can be used later during the approach to compute incorrect user (aircraft) position. To bound the possible position error caused by an ephemeris anomaly, we consider two limiting cases for cycle estimation implementations:

- *Limit Case 1:* Cycle ambiguities are established by averaging code against carrier.
- *Limit Case 2:* Cycle ambiguities are established using redundancy of carrier measurements.

Most implementations will use a hybrid of these two limiting scenarios.

3.1 Limit Case 1

In his scenario, known as 'geometry-free' cycle resolution, the ephemeris error does not affect yhe cycle ambiguity estimation process because averaging the difference of code and carrier to measure the cycle ambiguity is not dependent on satellite geometry information. However, given that the cycle ambiguities are correctly estimated, errors will still be incurred during the positioning process because satellite geometry information is used. Specifically, positioning error due to satellite ephemeris error will be proportional to the displacement between the aircraft and reference receiver. In Figure 11, the solid line qualitatively illustrates the erroneous vertical position error history over the flight path. The mathematical expression for vertical position error is:

$$\delta x = H_{3,i}^{+} \delta H_i \, u \, x \tag{3}$$

where H is the geometry matrix, H^{+} is its pseudoinverse, δH_i is the error in the geometry matrix due to an ephemeris error on satellite i, u is the approach path direction (unit vector), x is the scalar displacement between the aircraft and reference antennas, and δx is the resulting vertical position error due to orbit ephemeris error.

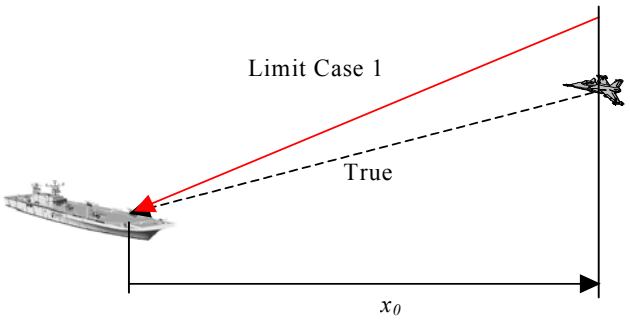

Figure 11. Vertical Position Error Due to Orbit Ephemeris Error For Limit Case 1

The relative residual used for detection is

$$\delta r \overset{\Delta}{=} r_0 - r = (I - HH^{+}) \delta H_i \, u \, \alpha x \tag{4}$$

where r_0 is the residual vector at the start (service entry) distance x_0, r is the residual vector at distance x, and the scalar factor α is defined as $(x_0 - x)/x$. Therefore at a given distance x, the observable effect of the ephemeris on the residual is magnified by the value of α. From a RAIM interpretation, as illustrated in Figure 12, the FMS will decrease as α increases.

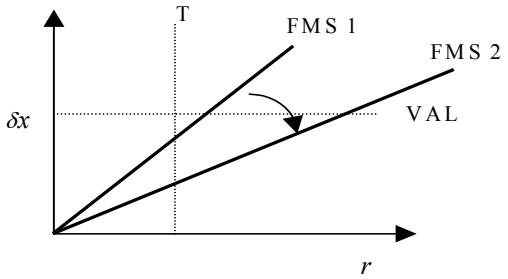

Figure 12. Effect of Increasing α

We will return to a discussion of the ramifications of the α parameter after Limit Case 2 is developed.

3.2 Limit Case 2

In this scenario, unlike Limit Case 1, orbit ephemeris errors do have an effect on the cycle ambiguity estimation process. In this case, the floating cycle ambiguity estimate for the affected satellite will absorb the effective ranging error induced by the ephemeris error. The resulting position error will be small near the effective cycle resolution distance (x_1) because the ephemeris error induced at this distance will be nearly cancelled by the error in the estimated cycle ambiguity. As the aircraft approaches the ship, however, the position error will increase proportionally with the displacement from the effective cycle resolution point (x_1–x). The maximum position error will occur the aircraft touch down point (x=0) as shown in Figure 13. The mathematical expression is for vertical position error in this case is

$$\delta x = H_{3,i}^{+}\delta H u x^{*} \qquad (5)$$

where $x^{*} = x_1 - x$, and x_1 is equivalent cycle resolution distance.

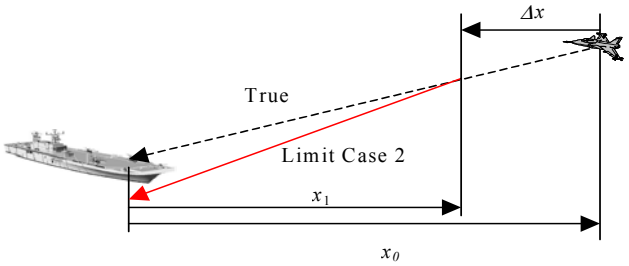

Figure 13. Vertical Position Error Due to Orbit Ephemeris Error For Limit Case 2

The relative residual can be computed using (6) whose form is identical to (4). The difference between two equations is simply that x has been replaced by x^{*} and the scalar factor α is in this case defined to be $(x_0 - x)/x^{*}$:

$$\delta r \overset{\Delta}{=} r_0 - r = (I - HH^{+})\delta H u \alpha x^{*} \qquad (6)$$

As qualitatively illustrated in Figure 14 for this limiting case, RAIM performance will improve as the distance x_0–x_1 increases because the relative residual will grow larger before the first erroneous CDGPS position fix occurs (at $x = x_1$).

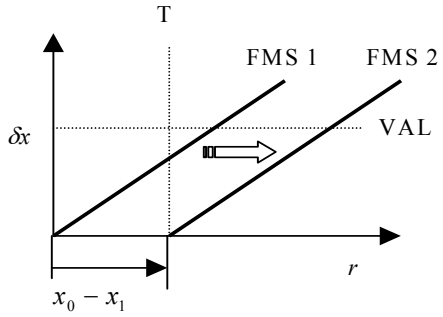

Figure 14 Effect on RAIM of increasing x_0–x_1

3.3 Availability of Ephemeris Fault Detection

Because the mathematical structures of equation sets (3)/(4) and (5)/(6) are identical, it is advantageous to consider both cases simultaneously. In particular, we are interested in the value of α that will result in RAIM availability of 99.7%. Recall as α increases, the residual will magnified relative to the position error for any given geometry; therefore RAIM availability will be improved. In this regard, Figure 15 shows the RAIM availability results as a function of α. These results assume the worst observed case Central Pacific ship location defined earlier, a missed detection probability of 10^{-4}, σ = 1 cm, and three different elevation mask angles. The quantitative results clearly show that as α increases, availability is improved. When α = 5, the 99.7% availability requirement is achieved. (Relatively modest additional gains in availability are achievable for $\alpha > 5$). We therefore define the desired value $\alpha_{des} = 5$.

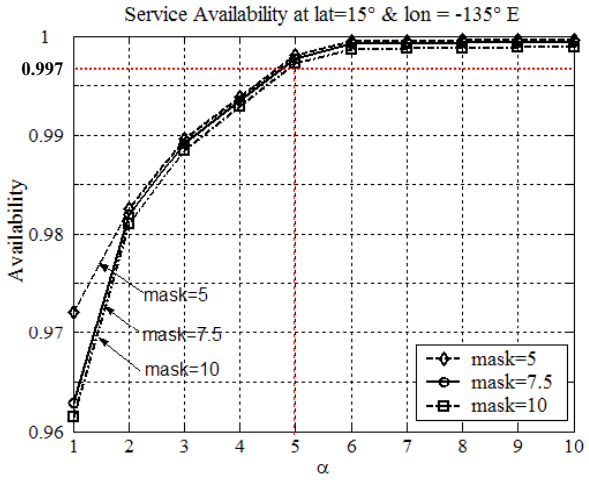

Figure 15. Service Availability of Orbit Ephemeris Detection

Although we want $\alpha \geq \alpha_{des}$ for each of the two limit cases, the interpretation of this result is different for each. Using

the definition of α for Limit Case 1, it is required that x be smaller than $x_0/(1+\alpha_{des})$ to ensure RAIM availability. (Conversely, for all distances in excess $x_0/(1+\alpha_{des})$ the RAIM function for ephemeris detection is not available with the desired missed detection performance.) Figure 16 shows, for several values of α, the maximum distance (x) within which RAIM is available as a function of the service entry distance (x_0). For example, given a service entry distance is 50 nmi, then RAIM-based ephemeris detection is 99.7% available (α = 5) within a radius of 8.33 nmi from the ship.

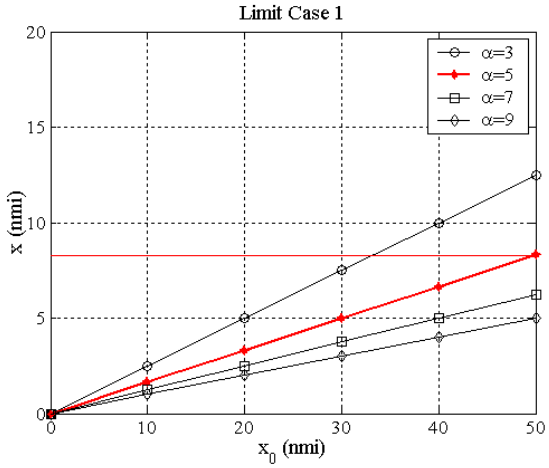

Figure 16. x vs. x_0 for Limit Case 1

Using the definition of α for Limit Case 2, it is required that x_1 (the effective cycle resolution distance) be smaller than x_0/α_{des} to ensure availability for all $x < x_1$. Figure 17 shows, for several values of α, the maximum effective cycle resolution distance (x_1) within which RAIM is available as a function of the service entry distance (x_0). For example, given a service entry distance is 50 nmi, then RAIM-based ephemeris detection is 99.7% available ($\alpha = 5$) for $x < x_1$, if x_1 is 10 nmi or smaller.

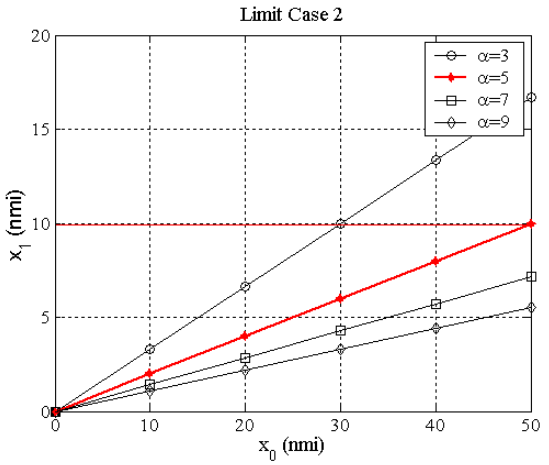

Figure 17. x_1 vs. x_0 for Limit Case 2

Table 2 summarizes the necessary conditions imposed by the two limit cases to achieve 99.7% availability ($\alpha = 5$) of the relative RAIM ephemeris fault detection function. Both conditions should be satisfied to ensure RAIM performance for operational SRGPS navigation architectures.

Required Service Availability	99.7% => α = 5	
Limit Case	1	2
Necessary Condition	$x < x_0/6$	$x_1 < x_0/5$

Table 2. Summary of Orbit Ephemeris Error Detection

4. IONOSPHERIC ERROR DETECTION

Nominally the effects of ionospheric errors are mitigated by the use of differential GPS. However, large ionospheric spatial gradients will cause differential ranging errors that are dependent on the displacement of the aircraft from the ship. (Such sharp gradients are rare, being relatively more common near the auroral and equatorial region where the highest values of range delay are expected.) In this regard the relative RAIM algorithm discussed above can also be effective against anomalous ionospheric gradients affecting a given satellite. Unfortunately, in contrast to ephemeris failures, ionospheric gradient anomalies can potentially occur on multiple satellites simultaneously. (This is not the case for orbit errors since ephemeris data for each satellite is uploaded independently and at different times.) Nevertheless, because dual frequency measurements will nominally be available with SRGPS, it is possible to use carrier phase measurements to directly detect anomalous ionospheric gradients in real-time during the aircraft approach. Moreover, the SRGPS user can also observe the anomalous ionospheric gradient with single frequency measurements (for example, when interference or jamming are present on one frequency). This is true because of the divergence effect of the ionosphere on code and carrier measurements. In this section, we consider an ionospheric threat model consisting of an anomalously large, constant spatial gradient during the approach. (More complex threat models, such as abrupt, non-linear changes in ionospheric delay during the approach, will be addressed in future work.) A means for autonomous detection of ionospheric spatial gradients will be described, and the effectiveness of the detection algorithms will be explicitly quantified.

4.1 Dual Frequency Gradient Estimation

Assuming a linear gradient model of the differential ionosphere is applicable for any given satellite, the magnitude of the gradient can be directly observed using dual frequency measurements taken over the aircraft approach. Taking the difference between L1 and L2 single difference carrier phase measurements when the aircraft is at a distance x from the reference station, we have for a given satellite

$$\Delta\phi_{L1} - \Delta\phi_{L2} = (1-\gamma_{12})kx + bias + \nu \tag{7}$$

where k is the differential L1 ionospheric gradient for the satellite, ν is the nominal measurement error (assumed to be normally distributed with standard deviation σ_ν), and γ_{12} is equal to $f_{L1}^2 / f_{L2}^2 = 1.65$. We can estimate the gradient by constructing measurement equation (7) at the service entry distance x_0 and some distance x (where $x < x_0$) later during the approach, differencing the results and dividing by $(\gamma_{12}-1)(x_0-x)$. The resulting ionospheric gradient estimate is distributed as

$$\hat{k} \sim N\left(k, \frac{\sigma_{\Delta I,dual}^2}{(x_0-x)^2}\right) \tag{8}$$

where $\sigma_{\Delta I,dual} = \frac{\sqrt{2}}{0.65}\sigma_\nu$.

4.2 Single Frequency Gradient Estimation

The ionospheric gradient can be also directly (but less precisely) estimated using single frequency measurements. Taking the difference between code and carrier single difference measurements when the aircraft is at a distance x from the reference station, we have for a given satellite

$$\Delta\rho - \Delta\phi = 2kx + bias + \nu_{\rho-\phi} \tag{9}$$

Following the process above, we estimate the gradient by constructing measurement equation (9) at the service entry distance x_0 and some distance x later during the approach, difference the results, and divide by $2(x_0-x)$. The resulting ionospheric gradient estimate is distributed as

$$\hat{k} \sim N\left(k, \frac{\sigma_{\Delta I,\rho-\phi}^2}{(x_0-x)^2}\right) \tag{10}$$

where $\sigma_{\Delta I,\rho-\phi} = \frac{\sqrt{2}}{2}\sigma_{\rho-\phi}$.

4.3 Effect of Ionospheric Gradient on Carrier Phase Positioning

As was the case with ephemeris failures, the existence of an anomalous ionospheric gradient may also affect the cycle ambiguity estimation process. In turn, incorrectly estimated cycle ambiguities can be used later during the approach to compute incorrect user (aircraft) position. To bound the possible position error caused by ionospheric gradient anomalies, we again consider the two limiting cases for cycle estimation already defined.

Let us assume that the effective cycle resolution distance is x_1 and the cycle resolution error due to the existence of the ionospheric gradient is δN. In this case, the effective single difference carrier ranging error experienced at a distance x from the ship is

$$\delta\phi(x) = -\delta N - kx \tag{11}$$

where nominal carrier phase measurement errors are neglected for the moment. The error in the cycle ambiguity, δN, will differ for the two limit-case cycle estimation scenarios. Table 3 shows the cycle ambiguity estimate errors along with the effective ranging error at $x = 0$ and $x = x_1$ computed from equation (11) for the two limiting cases. Figure 18 is an illustration of the corresponding position error histories. Because Limit Case 1 results in worse position errors throughout the approach, only this case will be considered in the analysis that follows.

	δN	$\delta\phi(0)$	$\delta\phi(x_1)$
Limit Case 1	$-2kx_1$	$2kx_1$	kx_1
Limit Case 2	$-kx_1$	kx_1	0

Table 3. Cycle Resolution and Effective Ranging Measurement Errors

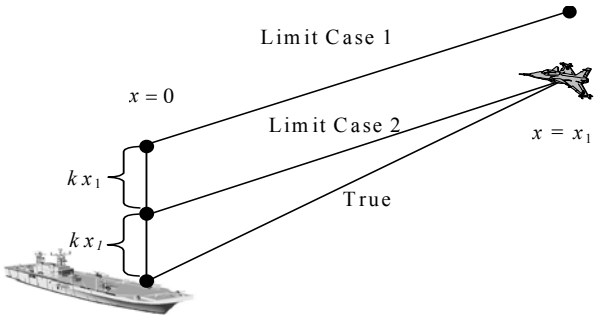

Figure 18. Illustrated Position Error Histories Due to Ionospheric Gradient

4.4 Autonomous Ionospheric Gradient Detection Performance

Substituting the value of δN for Limit Case 1 in Table 3 into ranging error equation (11), it is possible to write an upper bound on vertical position error as

$$\delta x = \left\| H^{+}_{3,:} \right\|_1 \cdot b \cdot \beta + v_x \qquad (12)$$

where the following definitions are relevant:

- $\left\| H^{+}_{3,:} \right\|_1$ is the 1-norm of $H^{+}_{3,:}$
- $b \equiv \dfrac{k_{\max}(x_0 - x)}{\sigma_{\Delta I}}$ (13)
- $\beta \equiv \dfrac{(2x_1 - x)}{x_0 - x}\sigma_{\Delta I}$.
- $k_{\max}$ is the maximum value of the ionospheric gradient for any satellite in view

The value of $\sigma_{\Delta I}$, defined just below equations (8) and (10), will depend on whether dual frequency or single frequency measurements are used to estimate ionospheric gradient. The normalized test statistic used for detection is

$$r \equiv \frac{\hat{k}_{\max}(x_0 - x)}{\sigma_{\Delta I}} = b + \tilde{v}_k \qquad (14)$$

where $\tilde{v}_k \sim N(0,1)$.

As the ionospheric gradient ($k_{\max}$) increases, b also increases, and both the position error (12) and the test statistic (14) become larger. In this case, we wish to find the value of β to attenuate the effect of b on position error such that the availability of the detection function meets the target requirements. The detection function availability results are plotted as a function of β in Figure 19. It is evident that for values of $\beta = 0.2$ or smaller that the availability is sufficient for the SRGPS application.

Given the definition of β in equation (13) and its required value to ensure availability (β = 0.2), we are able to define necessary conditions on cycle resolution distance as follows:

$$\frac{\beta}{\sigma_{\Delta I}} > 1: \quad \frac{x_1}{x_0} \le \frac{\beta/\sigma_{\Delta I}}{1 + \beta/\sigma_{\Delta I}} \qquad (15)$$

$$\frac{\beta}{\sigma_{\Delta I}} < 1: \quad \frac{x_1}{x_0} \le \frac{\beta}{2\sigma_{\Delta I}} \qquad (16)$$

These constraints are expressed graphically in Figure 20.

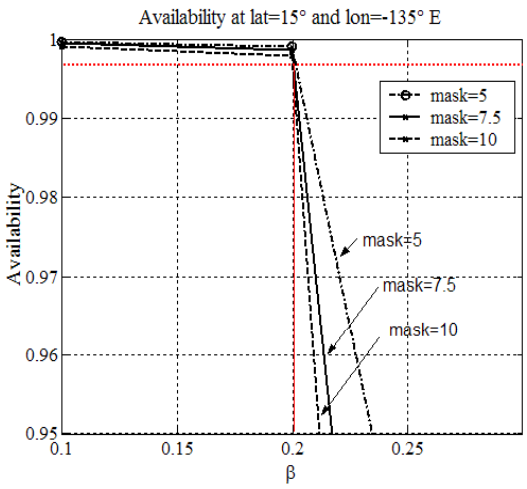

Figure 19. Service Availability vs. β

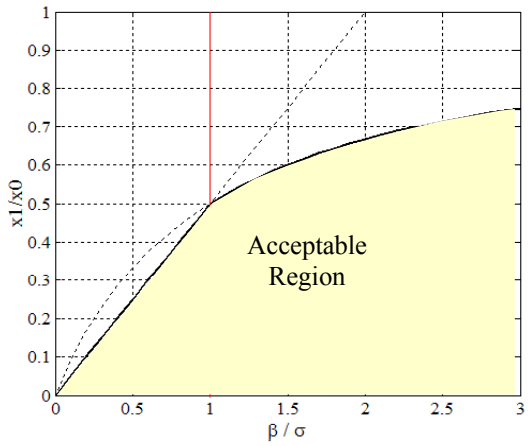

Figure 20. Constraint on Cycle Resolution Distance

As an example, given that $\sigma_{\Delta I,dual}$ (for the nominal dual frequency case) is 0.031 (m) and $\sigma_{\Delta I,\rho-\phi}$ (for the single frequency case) is 0.21 (m), together with a service entry distance (x_0) of 50 nmi, then hazardous ionospheric gradients are detectable when the effective cycle resolution distance (x_1) is less than 24 nmi for single-frequency case and 43 nmi for dual frequency. The results for other values of (x_0) are shown in Figure 21.

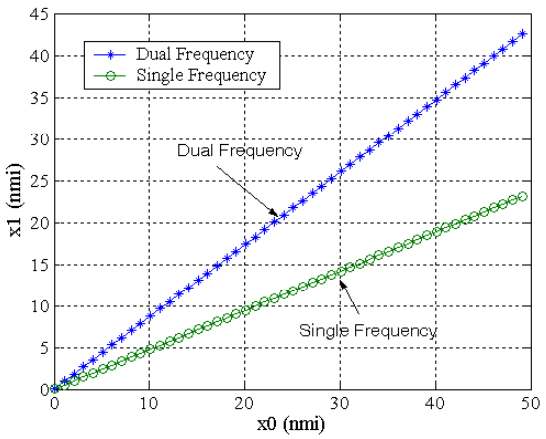

Figure 21. Maximum Effective Cycle Resolution Distance Constraint

5. CONCLUSION

This research is focused on the design of SRGPS airborne integrity monitor algorithms to detect and isolate navigation threats that are undetectable by integrity monitors at the shipboard differential reference station. Three specific navigation integrity threats were to be addressed in this work: airborne receiver cycle slips, orbit ephemeris anomalies, and ionospheric gradient anomalies

A RAIM-based cycle slip detection algorithm has been developed and evaluated using integer and half-integer constraints on failure magnitude. Based on the results, it is determined that while RAIM can be effective for specific threat models, the availability of the RAIM function is insufficient to protect against all classes of cycle slip threats. In this regard, it is recommended that RAIM-based cycle slip detection function be augmented in future work by integration of INS measurements.

A relative RAIM-based autonomous orbit ephemeris fault detection algorithm has also been developed, evaluated and shown to be sufficient to provide protection against ephemeris threats. Necessary conditions for operational distance requirements are specifically defined to ensure availability of the fault detection function.

Finally, autonomous ionospheric gradient detection algorithms have been designed using direct observation methods. Necessary conditions to ensure fault detection availability for both dual and single frequency implementations are defined.

6. ACKNOWLEDGMENTS

The authors gratefully acknowledge the U.S. Navy (Naval Air Warfare Center) for supporting this research. However, the views expressed in this paper belong to the authors alone and do not necessarily represent the position of any other organization or person.

7. REFERENCES

[1] Beser J. and Parkinson B. W., "The Application of NAVSTAR Differential GPS in Civilian Community," *NAVIGATION: Journal of Institute of Navigation*, Vol.29, No.2, Summer, 1982.

[2] Teasley S. P., Hoover W. M., and Johnson C. R., "Differential GPS Navigation," *Position, Navigation, and Location Symposium (PLANS 80),* Altantic City, New Jersey, December 1980.

[3] *Minimum Aviation System Performance Standards for The Local Area Augmentation System*, RTCA Paper No. 037-98/SC159-778, Feb. 1998.

[4] Kalafus R. M., "Receiver Autonomous Integrity Monitoring of GPS," Project Memorandum DOT-TSC-FAA-FA-736-1, U.S. DOT Transportation System Center, Cambridge, MA, 1987.

[5] Parkinson B. W. and Axelard P., "Autonomous GPS Integrity Monitoring Using the Pseudorange Residual," *NAVIGATION: Journal of Institute of Navigation*, Vol. 35, No2, pp. 255-274, 1988

[6] Pervan, B. and Parkinson, B. W., "Cycle Ambiguity Estimation for Aircraft Precision Landing Using the Global Positioning System," *Journal of Guidance, Control, and Dynamics*, Vol. 20, No.4, pp 681-689, 1997.

[7] Pervan, B. and Chan F., "System Concepts for Cycle Ambiguity Resolution and Verification for Aircraft Carrier Landings", *Proceedings of ION GPS-2001*, Salt Lake City, Utah, September 2001.

[8] *Global Positioning System Standard Positioning Service Signal Specification*, 2nd Edition, June 1995.

[9] Altmayer C., "Cycle Slip Detection and Correction by Means of Integrated System," Proceedings of ION NTM-200, Anaheim, CA, January 2000.

[10] Colombo O. L., Bhapkar U.V., Evans A.E., "Inertial-Aided Cycle-Slip Detection/Correction for Precise, Long-Baseline Kinematic GPS," *Proceedings of ION GPS-99*, Nashville, TN, September 1999.

[11] JPALS Test Planning Working Group, *Architechture and Requirements Definition: Test and Evaluation Master Plans for JPALS*, January 19, 1999.

[12] *Operational Requirements Document (ORD) for Joint Precision Approach and Landing System (JPALS)*, USAF 002-94-I.

[13] Koenig, M., Gebre-Egziabher D., Pullen S., Kim U.S., Pervan B., Chan, F.-C., "*Analysis of Reference Antenna Motion on the JPALS Shipboard Integrity Monitor*", ION NTM-2002, Anaheim, CA, January 2002.